euspen's 23rd International Conference & Exhibition, Copenhagen, DK, June 2023
www.euspen.eu

Effect of drawbar dynamics on tool point FRF of multipurpose aerostatic spindle

Jooho Hwang[1], Dang Chi Cong[1], Jongyoup Shim[1]

[1]*Department of Ultra-Precision Machines & Systems, Korea Institute of Machinery and Materials, 156, Gajeongbuk-Ro, Yuseong-Gu, Daejeon 34103, Republic of Korea*

jooho@kimm.re.kr

Abstract

Contact parameter in the high-speed spindle is an important parameter in tool point frequency response function (FRF) prediction, or receptance, which is the key factor in calculating the best operation condition of the spindle. In this paper, we describe an approach for the compensation tool and tool holder contact parameter by removing the effect of mass loading of an accelerometer used in the experiment process. The mass effect of the accelerometer is removed from tool point FRF by inversed Receptance Coupling Substructure Analysis (RCSA) before estimating the contact parameter. The result contact parameter was used to predict the tool point FRF of the spindle. The drawbar in the automatic tool change mechanism is coupled to the shaft of the spindle. The contact parameter of a tool holder and tool is evaluated from the experiment. The tool, tool holder, and shaft receptance were modeled by the Timoshenko beam theory. The fidelity of tool point FRF of spindle and stability lobe diagram after being predicted with the proposed method is improved.

FRF, Spindle, Modeling, Stability, Drawbar, RCSA,

1. Introduction

A key aspect of high-speed machining technology is the high-speed spindle, in particular, the high-speed spindle frequency response function, or FRF. Understanding the FRF of a spindle can prevent the spindle from running at critical speeds, provide higher stability during cutting, and avoid chatter through the use of stability lobe diagrams [1–4].

Aerostatic spindles are widely used to meet the increasing demand for fine finishing of surfaces by providing low friction for high-speed rotations. A drawbar is installed in the hollow spindle shaft of the automatic tool change (ATC) system of a multi-purpose spindle, e.g., the milling and finishing process only requires one spindle. Several researchers have investigated the effects of a drawbar on the dynamics of a spindle system [5], but they did not consider the tool holder or tool. Few researchers have studied the effects of a drawbar on the tool point FRF [6]. Neglecting the effects of a drawbar can have a detrimental effect on the estimation of the tool point FRF.

2. Modeling for tool point dynamics of aerostatic spindle

An aerostatic spindle can be modelled as an assembly of several substructures, as shown in Figure 1.

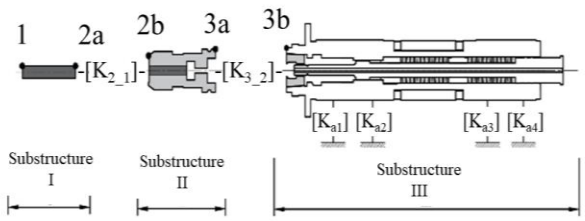

Figure 1. Models combined into the substructure of a spindle

In the model shown in Figure 1, Substructure I includes the flute and shank of the tool. Substructure II includes the tool-holder (i.e., the nut, collet, and tool shank for a collect connection). Substructure III includes the shaft, drawbar, and aerostatic bearings, with stiffness matrices $[K_{a1}]$, $[K_{a2}]$, $[K_{a3}]$, and $[K_{a4}]$. Note that the tapering component of the tool-holder is included in Substructure III. To estimate the dynamic response at the tool point, these three substructures were combined together with the aid of two contact parameters using the RCSA method[7-9].

A drawbar has a common neutral axis and is located inside a shaft. We used the four-point receptance coupling approach to describe the dynamic response of the combination of shaft and drawbar, as in [10]. These four points denoted as c1, c2, c3, c4 are the actual contact positions of the drawbar and the shaft; the structure is divided into three segments.

$$[\mathbf{G}_{3b3b}] = \frac{\mathbf{U}_{c1}}{\mathbf{Q}_{c1}} = \mathbf{R}_{c1c1}\frac{\mathbf{q}_{c1}}{\mathbf{Q}_{c1}} + \mathbf{R}_{c1c2}\frac{\mathbf{q}_{c2}}{\mathbf{Q}_{c1}} + \mathbf{R}_{c1c3}\frac{\mathbf{q}_{c3}}{\mathbf{Q}_{c1}} + \mathbf{R}_{c1c4}\frac{\mathbf{q}_{c4}}{\mathbf{Q}_{c1}} \quad (1)$$

The direct receptance of the shaft is represented as a Timoshenko beam model with aerostatic bearing dynamics $[K_{a1}]$, $[K_{a2}]$, $[K_{a3}]$, and $[K_{a4}]$; these were evaluated experimentally. The receptance of the drawbar was modeled as a Timoshenko beam model.

After taking into account the effects of the drawbar, we modelled the arbitrary tool-holder receptance (Substructure II) using Timoshenko beam theory, and then coupled it to the receptance of the shaft-drawbar assembly (Substructure III) using Equation (1):

$$[\mathbf{G}_{2b2b}] = [\mathbf{R}_{2b2b}] - [\mathbf{R}_{2b3a}]([\mathbf{R}_{3a3a}] + [\mathbf{G}_{3b3b}] + [\mathbf{K}_{3\_2}])^{-1}[\mathbf{R}_{3a2b}] \quad (2)$$

where $[K_{3\_2}]$ is the contact parameter between Substructures III and II. We then estimated the receptance based on our experimental results and the known value of the tool holder receptance. These processes will be explained in more detail in

the next section. The next step was to couple the tool (Substructure I) to the Substructure III-II assembly. The tool was modeled as a two-segment cylinder using Timoshenko beam theory. The parameter $[K_{2\_1}]$ is the contact parameter between Substructures II and I; we estimated this value experimentally and used the known value of the receptance of a two-segment cylinder.

$$[\mathbf{G}_{11}]=[\mathbf{R}_{11}]-[\mathbf{R}_{12a}]([\mathbf{R}_{2a2a}]+[\mathbf{G}_{2b2b}]+[\mathbf{K}_{2\_1}])^{-1}[\mathbf{R}_{2a1}] \quad (3)$$

The two contact parameters $[K_{3\_2}]$ and $[K_{2\_1}]$ and the four dynamical quantities characterizing each of the aerostatic bearings are evaluated in the next sections.

However, in reality the effect of the drawbar should also be taken into account. The contact parameter $[K_{3\_2}]$ can be calculated using Equation (3).

$$[\mathbf{K}_{3\_2}]=\left(\left([\mathbf{R}_{2b3a}]^{-1}([\mathbf{R}_{2b2b}]-[\mathbf{G}_{2b2b}])[\mathbf{R}_{3a2b}]^{-1}\right)^{-1}-[\mathbf{R}_{3a3a}]-[\mathbf{G}_{3b'3b'}]\right)^{-1} \quad (4)$$

In Equation (4), the term $[G_{3b'3b'}]$ represents the rigid combination of the shaft and drawbar receptances. The effects of the aerostatic bearing dynamics are not taken into account when using this method to determine $[K_{3\_2}]$, which has the following form:

$$[\mathbf{K}_{3\_2}]=\begin{bmatrix}\mathbf{k}_{xf}+i\omega\mathbf{c}_{xf} & \mathbf{k}_{xm}+i\omega\mathbf{c}_{xm}\\ \mathbf{k}_{\theta f}+i\omega\mathbf{c}_{\theta f} & \mathbf{k}_{\theta m}+i\omega\mathbf{c}_{\theta m}\end{bmatrix} \quad (5)$$

In Equation (6), four of the terms $[R_{2b'3a}]$, $[R_{2b'2b'}]$, $[R_{3a2b'}]$, $[R_{3a3a}]$ were obtained by applying the Timoshenko beam theory for the tool holder.

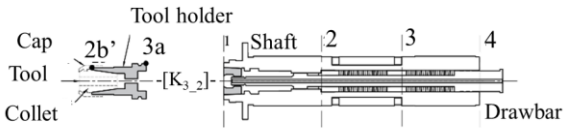

Figure 2. Evaluation of the contact parameter $[K_{3\_2}]$ between Substructures III and II

$$[\mathbf{K}_{3\_2}]=\left(\left([\mathbf{R}_{2b'3a}]^{-1}([\mathbf{R}_{2b'2b'}]-[\mathbf{G}_{2b'2b'}])[\mathbf{R}_{3a2b'}]^{-1}\right)^{-1}-[\mathbf{R}_{3a3a}]-[\mathbf{G}_{3b'3b'}]\right)^{-1}$$
$$[\mathbf{G}_{3b'3b'}]=[\mathbf{R}_{3b'3b',S}]-[\mathbf{R}_{3b'3b',S}]([\mathbf{R}_{3b'3b',S}]+[\mathbf{R}_{3b'3b',DB}])^{-1}[\mathbf{R}_{3b'3b',S}] \quad (6)$$

Up to now, we have not defined $[G_{2b'2b'}]$ when evaluating $[K_{3\_2}]$ in Equation (5) and Figure 2. This is the only term that has not been determined. In the following, we explain the term $[G_{2b'2b'}]$, which is the receptance of the free-free combination at point 2b' and has the form of Equation (7). Furthermore, we reduced the fluctuations in our calculations by applying this method to all of the FRFs measured:

$$[\mathbf{G}_{2b'2b'}]=\begin{bmatrix}\frac{\mathbf{X}_{2b'}}{\mathbf{F}_{2b'}} & \frac{\mathbf{X}_{2b'}}{\mathbf{M}_{2b'}}\\ \frac{\mathbf{\Theta}_{2b'}}{\mathbf{F}_{2b'}} & \frac{\mathbf{\Theta}_{2b'}}{\mathbf{M}_{2b'}}\end{bmatrix}=\begin{bmatrix}\mathbf{H}_{2b'} & \mathbf{L}_{2b'}\\ \mathbf{N}_{2b'} & \mathbf{P}_{2b'}\end{bmatrix} \quad (7)$$

where $X_{2b'}$ and $\Theta_{2b'}$ are the transverse deflection and rotation at point 2b', respectively; $F_{2b'}$ and $M_{2b'}$ are the force and moment at point 2b', respectively. $H_{2b'}$ is the experimentally measured receptance, which we obtained from the results of an impact test and then used to synthesize $[G_{2b'2b'}]$. In this experiment, the drawbar, shaft, and tool holder assembly were hung on an un-stretched cord. Theoretically, $H_{2b'}$ is the ratio of the transverse displacement and force to the frequency. We recorded the acceleration $A_{2b'}$ (m/s2) and hammer signal $F_{2b'}$ (N), which we then converted into the displacement per force ratio using Equation (8),

$$[\mathbf{H}_{2b'}](\mathbf{m}/\mathbf{N})=\frac{\mathbf{X}_{2b'}}{\mathbf{F}_{2b'}}=-\frac{\mathbf{1}}{\omega^2}\frac{\mathbf{A}_{2b'}}{\mathbf{F}_{2b'}}(\mathbf{m}/\mathbf{N}) \quad (8)$$

3. Estimation of the FRF of the aerostatic bearing spindle

We now present our results for contact parameters $[K_{3\_2}]$, $[K_{2\_1}]$, and the aerostatic bearing $[K_a]$. We also discuss the applications of these results for different cases.

In the first stage, we coupled the drawbar and tool holder to the shaft. We used a different tool holder, tool holder B (17.5 mm collet length), to couple the components to verify the contact parameter $[K_{3\_2}]$, which we estimated using tool holder A (27.5 mm collet length). Tool holders A and B are shown in Figure 3. The taper face and clamping conditions of all of the tool holders used in this study were the same.

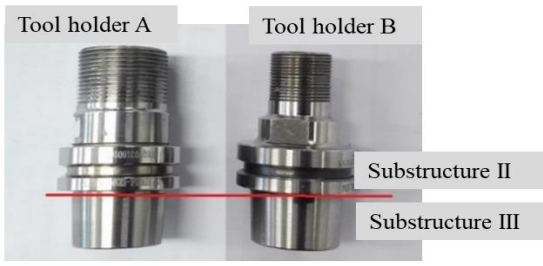

Figure 3. Tool holders A and B

The FRF at point 2b' in the case with the drawbar was estimated in a similar manner to Equations (1) and (2), taking the dynamics of the aerostatic bearings into account; we did not include the nut, collet, or tool inside the cap. We measured the FRF at point 2b' and the results are shown in Figure 4(a). The estimation of H_{2b}' at the end point of tool holder A based on the contact parameter obtained with the drawbar was better than the estimate obtained when using the contact parameter calculated without taking the drawbar into account. The reason for this is that the receptance of the drawbar was included in that of the shaft when using the multipoint receptance approach. The estimated contact parameter $[K_{3\_2}]$ calculated using tool holder A was used to estimate the displacement-to-force receptance $H_{2b'}$ of tool holder B, and the results are shown in Figure 4(b).

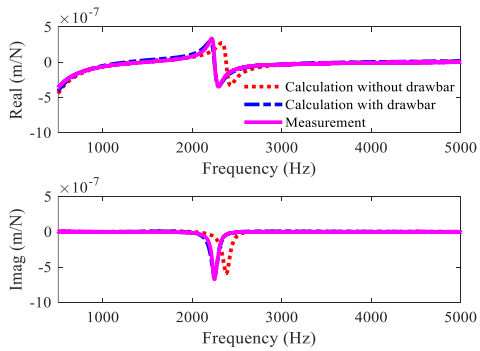

(a) FRF of $H^{2b'}$ with tool holder A

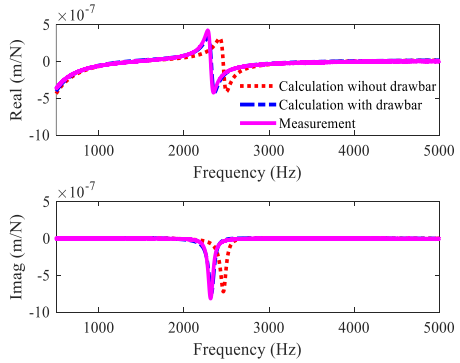

(b) FRF of $H^{2b'}$ with tool holder B

Figure 4. Comparison between the calculated (with and without the drawbar) and measured FRF at point 2b

In this section, we present the results of our analysis of the aerostatic bearings and our estimation of the tool holder end point FRF, taking into account the effect of the aerostatic bearings and drawbar. We estimated the results for the aerostatic bearings at air pressure 0.5 MPa then used this estimate to predict the corresponding values at 0.4 and 0.6 MPa. The cases of 0.4 and 0.6 MPa were similar to the case at 0.5 MPa.

Figure 5 shows the effects of the axial pulling force and the air pressure on the natural frequencies. The NF plane of tool holder A was lower than that of tool holder B due to A's larger size.

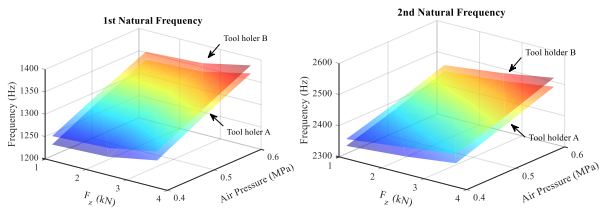

Figure 5. Difference between tool holder A and tool holder B with respect to the NF, while varying the clamping force F¬z and the air pressure (left: 1st NF, right: 2nd NF)

We then included the nut, collet, and tool inside the collet in our calculation. This enabled us to estimate H_{2b}, the FRF at point 2b. We calculated the full receptance [G_{2b2b}] both with and without the drawbar. This calculation procedure was similar to the receptance calculation used in the RCSA method, which was described in [11] . These receptance values, [G_{2b2b}], were used in the next sections of our study.

4. Effects of the drawbar on the tool point FRF of aerostatic bearing spindle

We applied Equation (6) with the values of the contact parameters [K_{2_1}] and [G_{2b2b}] and estimated the FRF of the tool point. We used tool holder A for these calculations. In the measurement procedure, the blank tool was clamped to the tool holder of the spindle and the spindle was placed on foam to resemble free-free condition.

The results of the coupling calculations and measurements are shown in Figure 6. We show the tool point FRF with a tool length of 32.5 mm on the left. We used this tool blank to estimate [K_{2_1}], and then repeated the estimation with a tool of length 42.5 mm, the results of which are shown on the right. Both carbide tools had a diameter of 6 mm. The estimation of the FRF was more accurate when the drawbar was included than when it was omitted. This is because in the previous coupling stage, the model without the drawbar provided a higher estimate in the second NF mode. Consequently, the NF of the tool without the drawbar was higher than that of the with-drawbar case. By including the drawbar in our model, we reduced the percentage error of in the tool mode NF to 1.3%, which is better than the 3.7% error obtained when the drawbar was not taken into account.

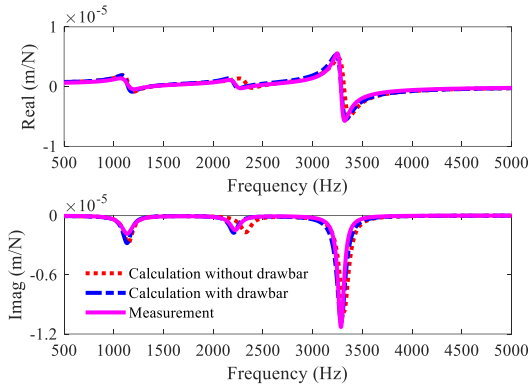

(a) 32.5 mm tool blank

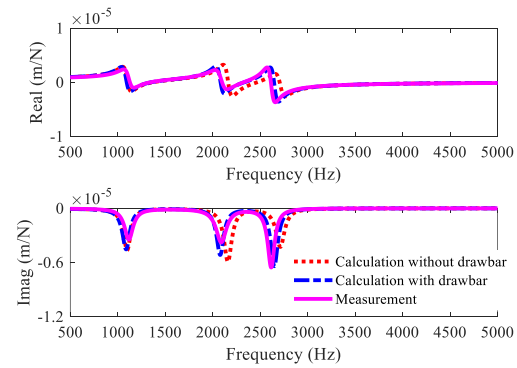

(b) 42.5 mm tool blank

Figure 6. Comparison between the calculation with and without the drawbar and measurement of the tool point FRF (a) 32.5 mm tool blank, (b) 42.5 mm tool blank

We estimated the stability lobe diagram (SLD) based on the FRF of the aerostatic spindle (Figure. 8) with the 42.5 mm tool blank clamped to tool holder A (Figure. 4). For the SLD calculation, the tool was assumed to have three flutes; the spindle to run clockwise; the milling type was set to face-milling; the feed rate was 0.2 mm/flute; and the work piece was chosen as aluminium 7050-T7451. The SLDs of the FRF were calculated for three different cases and the results are shown in Figure 7. We calculated the stability based on the FRF with the drawbar and found it to be much improved with respect to the depth of cut and spindle speed. These improvements did not only apply to low-speed operation (left) but were also observed in the case of high-speed operation (right), as shown in Figure 7. For example, when the spindle ran at 19,500 rpm, as shown on the right in Figure 7, the estimated SLD of the FRF without the drawbar implied that the spindle operation was stable until the depth of cut reached 1.8 mm. Meanwhile, the SLD of the FRF with the drawbar implied that the spindle operation was stable until the depth of cut reached 1.15 mm; this result is closer to the estimated SLD of the measured FRF (1.1 mm). Furthermore, for the lobe occurring at 17,000 ~ 30,000 rpm, the lowest depth of cut predicted by the FRF without the drawbar was 1.576 mm at 20,320 rpm; this is equivalent to a 42% error in the depth of cut for the measured FRF (1.104 mm) at 19,450 rpm. Meanwhile, the lowest depth of cut predicted by the FRF with the drawbar (1.138 mm) at 19,710 rpm differed from the depth of cut predicted based on

the measured FRF by only 3%. Moreover, the right-hand side of Figure 7 shows that the SLD predicted based on the FRF with the drawbar was better than the SLD predicted by the FRF without the drawbar at high spindle speeds (35,000 to 120,000 rpm).

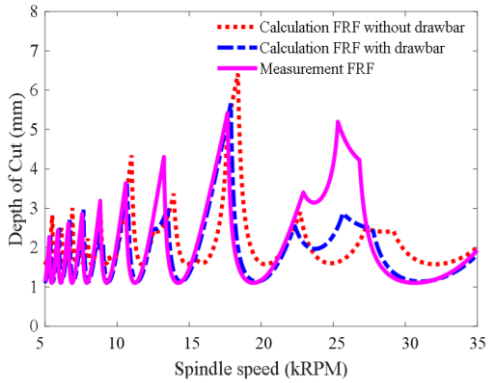

(a) Low spindle speeds

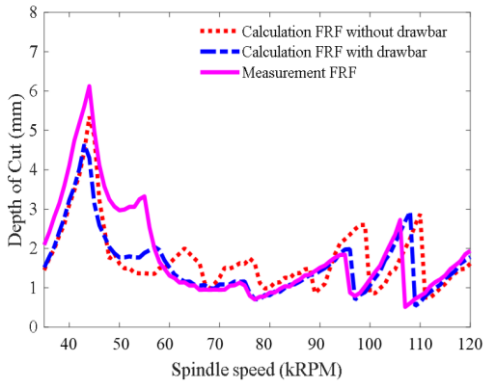

(b) High spindle speeds

Figure 7. Comparison between the results of the calculation without and with the drawbar and measurements over the stability lobe diagram at low spindle speeds (a) and high spindle speeds (b)

We validated our calculations by investigating the effects of tool length on the NF of the spindle, as shown in Figure 8. As expected, as the tool length varied, the third NF or tool natural frequency varied most, even when the conditions of the drawbar were varied. In this case, the minus sign "-" in "-10 mm" indicates that the current drawbar length was reduced by 10 mm and vice versa. The length of the last portion of the drawbar shown in Figure 2 was varied between -10 mm and 40 mm in increments of 10 mm.

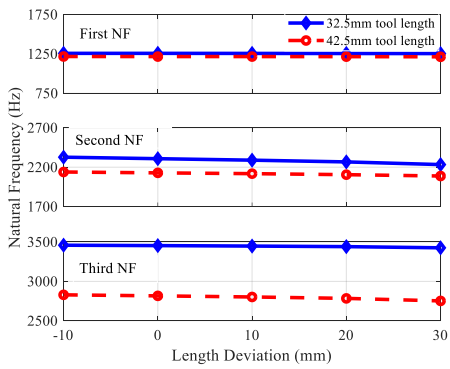

Figure 8. Effects of tool length on the natural frequency of the tool point of the aerostatic bearing spindle

5. Conclusions

In this study, we presented a novel method for predicting the tool point FRF of a multipurpose aerostatic spindle. We obtained better estimates of the FRF by including the drawbar. We estimated the tool point FRF by applying Timoshenko beam theory to calculate the receptances of the tool, tool holder, and shaft. We coupled the tool holder to the shaft and confirmed that the FRF at the endpoint of the tool holder was predicted accurately, with an NF error of 0.4%. We also coupled the tool to the tool holder and the shaft and obtained results that were in good agreement with the measured tool mode frequency data, with a percentage error of 1.7%. Therefore, this method is suitable for use by spindle designers when they are investigating the properties of spindles prior to production. This is the first time that two contact parameters, namely those between the shaft and the tool holder and the tool holder and the tool, have been included simultaneously in a tool point FRF calculation. This method corrects the NF of the spindle system before coupling it to the tool by using a better estimate of the contact parameter between the shaft and tool holder; hence, the tool mode frequency is expressed appropriately after coupling an arbitrary tool to the spindle system. Furthermore, our method corrects the receptance at frequencies of different modes, resulting in better estimations. In addition to the contact parameters, we also took into account the dynamics of the aerostatic bearings in the tool point receptance calculation. Thus, our calculation provided a good estimate of the tool point FRF of the spindle. We also estimated the SLD, emphasizing the importance of the inclusion of the drawbar when estimating the spindle dynamics. We also investigated the effect of the length and density of the drawbar and found that, although these do not affect the first NF of the spindle, they do affect the second, and especially the third NF. This information will be important to researchers studying machining. Therefore, it is beneficial to include the drawbar during the optimization stage of the design process.

References

[1] Tobias W and Fishwick S 1958 Theory of regenerative machine tool chatter *The Engineer* **205** 199-203

[2] Tlusty J 2000 *Manufacturing Processes and Equipment* (Upper Saddle River, NJ Prentice Hall)

[3] Budak E and Altintas Y 1998 Analytical Prediction of chatter stability in milling- part I: general formulation *J. of Dyn. Syst. Meas. Control* **120** 22-30

[4] Budak E and Altintas Y 1998 Analytical prediction of chatter stability in milling - part II: application of the general formulation to common milling system *J. of Dyn. Syst. Meas. Contro* **120** 31-36

[5] Jiang S and Zheng S 2010 A modeling approach for analysis and improvement of spindle-drawbar-bearing assembly dynamics *Int. J. Mach. Tools Manuf.* **50** 131-142

[6] Özşahin O Ertürk A Özgüven H and Budak E 2009 A closed-form approach for identification of dynamical contact parameters in spindle-holder-tool assemblies *Int. J. Mach. Tools Manuf.* **49** 25-35

[7] Schmitz T Davies M and Kennedy M 2001 Tool point frequency response prediction for high-speed machining by RCSA *J. Manuf. Sci. Eng.* **123** 700-707

[8] Schmitz T Predicting high-speed machining dynamics by substructure analysis 2000 *CIRP Ann. - Manuf. Technol.* **49** 303-308

[9] Schmitz T Powell K Won D Duncan G, Gregory W and Ziegert J 2007 Shrink fit tool holder connection stiffness/damping modeling for frequency response prediction in milling *Int. J. Mach. Tools Manuf.* **47** 1368-1380.

[10] Schmitz T and Smith K 2012 *Mechanical Vibrations* (London Springe)

[11] Kumar U Schmitz T 2012 Spindle dynamics identification for receptance coupling substructure analysis *Precis. Eng.* **36** 435-443